J Sol-Gel Sci Technol (2017) 84:475–485
DOI 10.1007/s10971-017-4451-7

INVITED PAPER: NANO- AND MACROPOROUS MATERIALS (AEROGELS, XEROGELS, CRYOGELS, ETC.)

Effect of freeze-drying parameters on the microstructure and thermal insulating properties of nanofibrillated cellulose aerogels

Clara Jiménez-Saelices[1,2,3] · **Bastien Seantier**[1] · **Bernard Cathala**[2] · **Yves Grohens**[1]

Received: 25 January 2017 / Accepted: 12 June 2017 / Published online: 20 June 2017

Abstract Nanofibrillated cellulose aerogels are low-density bio-based materials that present a great potential in several fields. The properties of aerogels are a consequence of their microstructure. The understanding and control of the structure is therefore a priority for the preparation of aerogels with specific properties. This study aims at investigating how freeze-drying conditions affect the microstructure of nanofibrillated cellulose aerogels and how their microstructure affects their thermal insulating properties. TEMPO-oxidized nanofibrillated cellulose aerogels were prepared by freeze-drying using two different moulds in order to vary the cooling rate and the temperature gradient. The microstructure of the nanofibrillated cellulose aerogels obtained was investigated using both scanning electron microscopy and nitrogen adsorption–desorption. Controlling solvent solidification has a drastic effect on aerogel microstructure. Different temperature gradients result in different distributions of pore size, each with its specific shape and connectivity. The thermal insulation properties of aerogels were evaluated using the hot strip technique. The resulting original structures revealed very different thermal insulation properties. Aerogels with a lamellar microstructure oriented in the direction of the temperature gradient showed porous channels. As a consequence, they had the poorest performance in terms of thermal insulating properties, with a minimal thermal conductivity of 0.038 W/(m·K). Aerogels with a cellular microstructure had smaller pores and reached a minimal thermal conductivity of 0.024 W/(m·K).

Graphical Abstract

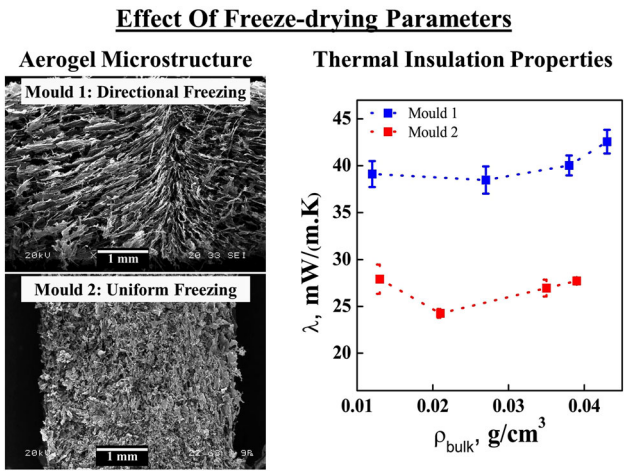

Keywords Nanofibrillated cellulose (NFC) · Aerogel · Freeze-drying · Nanostructure formation · Thermal insulation

✉ Clara Jiménez-Saelices
clara.jimenez-saelices@inra.fr

[1] IRDL, UBS, FRE CNRS 3744, Lorient 56100, France

[2] UR1268 Biopolymères Interactions Assemblages, INRA, Nantes 44316, France

[3] Agence de l'environnement et de la Maîtrise de l'Energie, 20, avenue du Grésillé, BP 90406, Angers 49004, France

1 Introduction

Cellulose nanofibers (NFCs) were introduced in the early 1980s by Turbak [1] and Herrick [2]. They produced cellulose fibres with nanometric lateral dimensions by treating softwood pulp aqueous suspension using a high-pressure

homogenization process. Depending on the treatment conditions, the NFCs have a diameter from 5 to 50 nm and a length of several micrometres [3]. In all cases, NFCs have crystalline and amorphous domains and a very high aspect ratio, giving them remarkable mechanical properties. Due to their particular properties, NFCs are used for a wide range of applications such as optically transparent materials [4, 5], reinforcements for nanocomposites [6, 7], high-performance multifunctional fibres [8], chiral nematic mesoporous materials [9] and insulation materials [10–12]. They have also attracted considerable interest as building units for the preparation of aerogels [10, 11, 13–17].

Aerogels are porous materials derived from gels for which the liquid phase has been replaced by a gaseous phase without destruction of the gel solid network [18]. NFC aerogels are among the lightest porous materials known at this time: they can reach densities of between 0.004 and 0.02 g/cm^3 [10, 11]. These densities are much lower than for cellulose aerogels because NFCs create three-dimensional structures at very low concentrations. Moreover, this structure is sufficiently resistant to counteract the collapse often observed during drying [11]. NFC aerogels therefore constitute low-density bio-based materials with high mechanical [19, 20] and thermal insulation properties [10, 12], presenting a great potential in several fields. The properties of aerogels are a consequence of their microstructure. Consequently, the use of a specific aerogel for a particular application requires a proper understanding and control of its structure. Supercritical drying preserves the three-dimensional structure during drying. The aerogels prepared using this method have a fibrillary morphology with a very small pore size and a very high surface area [10]. Aerogels prepared by freeze-drying have a film-like morphology with macropores and a very low specific surface area [13, 19, 21–23].

However, freeze-drying of porous materials has received a great deal of attention over the past few years. This simple process, where a material suspension is simply frozen and then sublimated, provides materials with unique porous architectures where the porosity is almost a direct replica of the frozen solvent crystals. Studies of various materials including ceramic [24] and metallic [25] particles reveal that the ice formation process has a critical role in determining the final microstructure of the porous materials. The porous structure is primarily defined by the morphology of the growing solvent crystals and, secondarily, by the ability of the particles to pack between the crystals since smaller particles will provide a better replica of the solvent crystals [26]. This technique can therefore be used to obtain hierarchically structured aerogels with interesting physical properties from aqueous dispersions of cellulose nanofibers. The freezing of NFC water suspensions was generally achieved by dipping them into liquid nitrogen baths or by placing them inside freezers. Some recent studies investigated the effect of the freezing direction on the structural characteristics of NFC aerogels [20, 27–29]. The unidirectional freezing of the aqueous suspension, followed by the unidirectional growth of ice crystals and the sublimation of ice crystal templates, results in highly ordered porous aerogels with unidirectional channels. This architecture can be useful in various applications such as the preparation of aligned pores in batteries [30] or liquid purification applications that favour directional capillary ascension [31, 32]. Similarly, the anisotropy is interesting for the preparation of porous scaffolds. Due to their biocompatibility, polysaccharides are widely used for the preparation of scaffolds in tissue engineering [33]. The tissue supports must have a high porosity and a large pore size (higher than 100 µm), as well as an interconnected structure for the transport of cells and metabolites [34].

The correlation between the microstructure and the mechanical properties of aerogels and foams has been investigated in the past few years. However, to the best of our knowledge, the effect of unidirectional freezing on the microstructure and thermal insulation properties of NFC aerogels has not. Thus, the objectives of this study were to investigate the effect of the processing conditions on the microstructural and thermal insulation properties of NFC aerogels. TEMPO-oxidized NFC suspensions were frozen at −80 °C inside different moulds in order to vary the cooling rate and the temperature gradient. The establishment of the temperature gradient inside the moulds was investigated by thermal transfer simulation. The microstructure of the NFC aerogels obtained was investigated using both electron microscopy and nitrogen adsorption–desorption. Their thermal insulation properties were evaluated using the hot strip technique. The resulting original structures showed very different thermal insulation properties.

2 Materials and methods

2.1 Materials

A 1 wt% aqueous suspension of NFC produced by TEMPO-mediated oxidation [35] of spruce wood pulp was received from the Swiss Federal Laboratories for Materials Science and Technology (EMPA, Dübendorf, Switzerland). The suspension was further characterized in order to confirm the supplier specifications. The 1.12 mmol/g carboxylate content was confirmed by conductimetric titration (SCAN-CM65:02, 2002). The dimensions were determined by atomic force microscopy (AFM) with a multimode setup equipped with the nanoscope III-a (Brucker-nano, Santa Barbara, CA, USA). The AFM was used in contact mode

imaging and the diameter and the length of the NFC were analyzed from 100 images. The height of the NFC was considered to estimate the lateral dimension of the NFC and was found to be approximately 3.85 ± 0.98 nm. A minimum length of 450 nm was determined. Both values are in good agreement with the EMPA's specifications.

2.2 Methods

2.2.1 Aerogel preparation

Bioaerogels were prepared via the concentration–drying route. Concentrations of NFC dispersions were achieved by osmotic concentration using dextran solutions. NFC dispersions were placed in a dialysis membrane, Espectra/Por®, with a cutoff of 12 to 14 kDa, and the dialysis membrane was immersed in a dextran solution at 10 wt%. Dextran is a complex branched glucan with a high molar mass, in this case, 100,000 g/mol. During this process, the dextran solutions are changed every 30 h. Final concentrations of hydrogels varied from 1 to 3 wt%. The suspensions were then freeze-dried (FD). NFC suspensions were frozen in a deep-freezer at −80 °C and then dried for 48 h using a Christ Alpha 1–2 LD Plus freeze-dryer. During freeze-drying, the condenser temperature was below −50 °C and the vacuum was below 0.1 mbar.

2.2.2 Thermal transfer simulation

Simulations were investigated using Comsol Multiphysics 5.1 software in order to check the establishment of the temperature gradient inside the moulds. For this purpose, the materials that make up the moulds, their dimensions and their thermal properties were defined. Simulation was carried out with water inside the mould to simplify the model. The initial temperature for mould and water was fixed at 20 °C, and a temperature of −80 °C was determined for the outer limits of the mould. The temperature variation produced by heat conduction during freezing was then analyzed as a function of time.

2.2.3 Characterization

The rheological measurements were conducted using a controlled-stress rheometer (Physica MCR 301, Anton Paar GmbH, Stuttgart, Germany) equipped with a parallel-plate geometry (PP25, 25 mm in diameter). Before each measurement, the samples were allowed to rest for 5–10 min. Before taking the dynamic viscoelastic measurements, the linear viscoelastic region was determined by torque sweeps for all suspensions. The torque sweeps were measured for 0.01 to 100 Pa at a frequency of 1 Hz. The chosen dynamic strain amplitude for the frequency sweep measurements was 0.1% for all suspensions since they showed linear viscoelasticity. The frequency sweeps were carried out in the range of 0.01–10 Hz at the linear viscoelastic region. The effect of temperature on gel properties was studied for ambient temperature. Rheological measurements were made in triplicate and the average was recorded. Data were recorded with Rheoplus software, version 3.62 (Anton Paar Germany GmbH).

Bulk density ρ_{bulk} of the aerogels was calculated by dividing their weight by their volume, which was measured by a digital caliper. The weight of aerogels was determined with an analytical balance (Mettler Toledo XS). In addition to this, porosity was calculated using Eq. 1, where the ratio $\rho_{bulk}/\rho_{skeletal}$ is the relative density. Skeletal density $\rho_{skeletal}$ is the density of cellulose: 1.6 g/cm^3 [36].

$$\varepsilon(\%) = (1 - (\rho_{bulk}/\rho_{skeletal})) \times 100 \quad (1)$$

A JEOL JSM 6460LV scanning electron microscope operating at 20 kV was used to capture structural images of the bioaerogels. Thin layers of gold were deposited by sputtering with scan-coat onto the surface of the cross-sections. Aerogel samples were prepared for scanning electron microscope (SEM) observation by cryo-fracture in liquid nitrogen. Image analysis was used in order to obtain more information about the pore structures from microscopical images. SEM images were evaluated with Image J, and the measurement of more than 100 pores in these images was used to obtain an approximate distribution of the pore size of each aerogel.

Nitrogen adsorption–desorption isotherms were obtained using a Micromeritics TriStar 3000 apparatus. Before running adsorption isotherm experiments, bioaerogel samples were degassed to remove all the species that can be physisorbed at their surface. During the experiments, samples were placed in a high vacuum at 100 °C for 24 h. The measuring cell was then placed in an insulated tank filled with liquid nitrogen that maintained the sample at −196 °C throughout the measurement, a temperature at which gaseous nitrogen adsorption is possible on a solid surface. A nitrogen adsorption-desorption isotherm represents the evolution of the volume of nitrogen adsorbed per gram of sample extrapolated to standard conditions of temperature and pressure (cm^3/g STP), depending on the relative pressure of nitrogen (P/P_0). Using the BET theory [37], it is possible to evaluate the specific surface area.

Thermal conductivity, λ, of the sample was measured in the steady state using the hot strip technique. This device, adapted from the hot filament technique, was previously developed for thermal characterization of aerogels [38, 39]. The hot strip technique (Fig. 1) consists of a homemade device comprising an isothermal aluminium case (Fig. 1d) with two cavities, one containing a polyurethane foam (Fig. 1b) and the other containing the sample to be

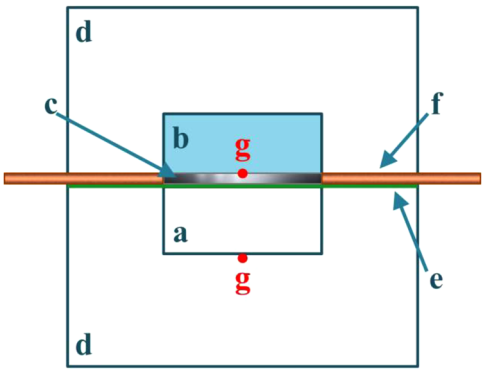

Fig. 1 Hot strip device: **a** Sample; **b** Polyurethane foam; **c** NiCr strip; **d** Isothermal aluminium case; **e** Electrical insulator; **f** Electrodes (copper); and **g** Thermocouples

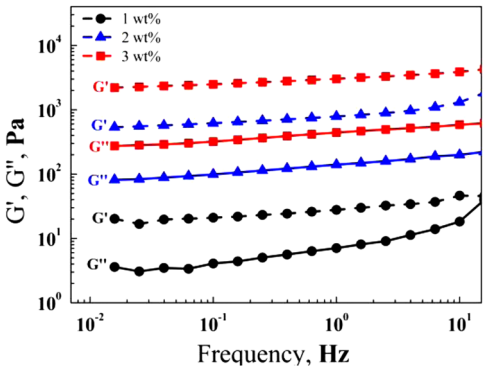

Fig. 2 Storage modulus G′ (*dashed lines*) and loss modulus G″ (*solid lines*) as a function of frequency for three concentrations of aqueous NFC suspensions

characterized (Fig. 1a). These two cavities are symmetrically positioned with respect to a strip (Fig. 1c) that is electrically isolated from the case (Fig. 1e). Two electrodes (Fig. 1f) provide the electrical power supply to the strip and two thermocouples (Fig. 1g) measure the temperature of both the strip and the case while the temperature of the case is kept constant by a cooling circuit.

The tests were performed at atmospheric pressure in a temperature- and humidity-controlled room (21–22 °C and 50% relative humidity). At least five samples per formulation were tested.

3 Results and discussion

3.1 Rheological characterization of hydrogels

NFC gelation is due to the physical entanglement of nanofibers and should thus result in viscoelastic behaviour. The viscoelastic behaviour of the aqueous suspensions of NFC with increasing concentration was studied by rheology. In classical viscous fluids, the elastic and loss modulus have a characteristic frequency dependency, i.e., $G' \propto f^2$ and $G'' \propto f^1$, where $G' \ll G''$. An ideal gel behaves elastically and $G' \propto f^0$, i.e., the storage modulus is independent of the frequency and $G' \gg G''$ [40]. On the basis of Fig. 2, a gel-like behaviour was observed for all of the NFC suspensions investigated, even for the lowest concentration. The conservation modulus G′ and the loss modulus G″ were relatively independent of the frequency at all of the concentrations investigated and, in all cases, $G' \gg G''$ up to a frequency of 10 Hz. In addition, the elastic moduli are almost 10-fold higher in comparison to the loss moduli at the same concentration, indicating that the network formed by the NFC is a strong network [41] due to hydrogen bonds. An increase in the concentration of 1 to 3 wt% results in a storage modulus that is 1000 times higher, which shows that G′ strongly depends on the concentration and intermolecular interactions.

3.2 Preparation of bioaerogels

Bioaerogels were prepared from suspensions of various NFC concentrations by FD. The process consists of two major steps: the freezing and the drying by sublimation of frozen water. The NFC suspensions were poured into different shaped moulds at room temperature and then placed in a deep-freezer at −80 °C for 24 h. Freeze-drying of the solvent created the final porous structure as a replica of the ice crystals generated during freezing. The moulds described below were therefore designed in such a way as to create different thermal transfers in the cast sample during the freezing stage.

Two moulds were designed to obtain different temperature gradients in order to obtain a gel-freezing pattern. The two moulds were designed so as to produce unidirectional (mould 1) and multidirectional (mould 2) freezing gradients. Mould 1 was a modular mould composed of three parts: two flat covers (100-mm long and 100-mm wide) made from high thermal conductivity aluminium ($\lambda = 200$ W/(m·K)), and a central piece in the shape of a "u" made from polypropylene ($\lambda = 0.2$ W/(m·K)) that determines the final thickness of the sample (Fig. 3a). The assembly is kept closed with screws. The samples prepared with this mould measure 80 × 80 mm and have a thickness of 10 mm. Mould 1 was designed in order to produce a temperature gradient in the sample during the freezing step. A simulation of conductive thermal transfer inside this mould was carried out using Comsol Multiphysics 5.1 software. The initial temperature was fixed at 20 °C for the mould as well as for the water filling the mould. A temperature of −80 °C was then determined for the outer limits of the mould and the temperature variation of the assembly was analyzed as a function of time. Figure 4 shows a selection of cross-section

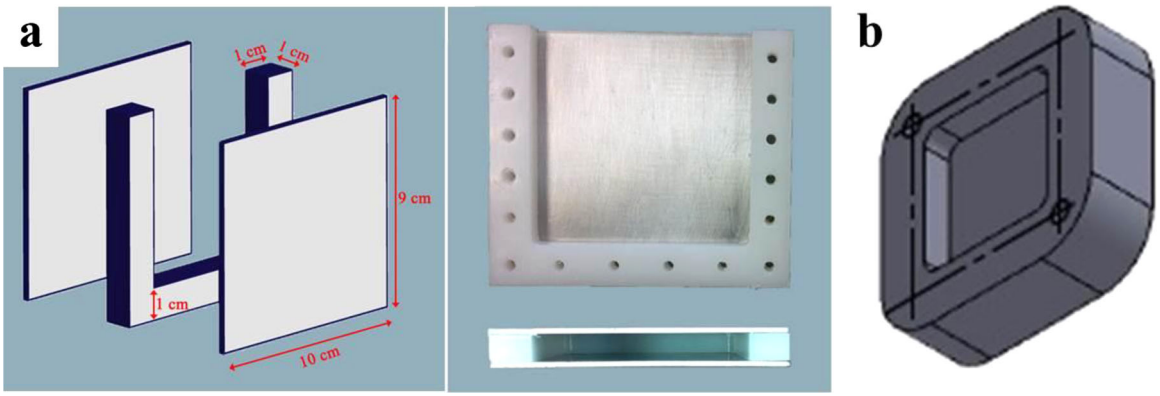

Fig. 3 **a** Diagram showing the different parts of mould 1 and its image. **b** Design of mould 2

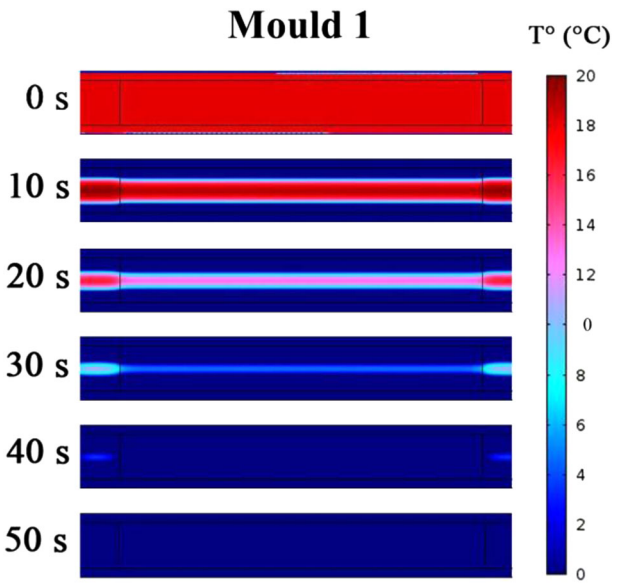

Fig. 4 Comsol simulation in two dimensions of the temperature gradient during the freezing of the samples in the mould 1. In the *red zone*, T° = 20 °C; in the blue zone, T° = 0 °C

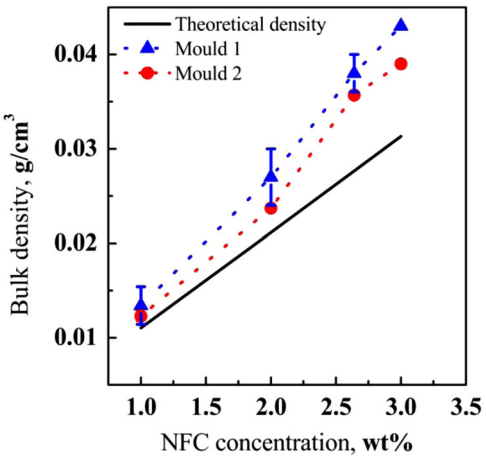

Fig. 5 Bulk densities of bioaerogels. *Dotted lines* show the dependence of bulk density on concentration. The *solid black line* is the theoretical density, which is calculated assuming that there is no volume shrinkage

aerogel images as a function of time. The colours represent the temperature, given that 20 °C is the initial temperature (*red*) and 0 °C is the final temperature (*blue*).

The temperature gradient describes the direction and intensity of the temperature variation between the cold source and the hot source. This is an important parameter because the growth of the crystals from the nuclei formed during the primary nucleation takes place in the direction of this gradient. The geometry and composition of the mould defines a temperature gradient going from each aluminium cover towards the inside of the sample.

Mould 2 was made entirely from high thermal conductivity aluminium ($\lambda = 200$ W/(m·K)) to produce a multidirectional freezing of NFC suspension (Fig. 3b). In addition, this mould is thinner in order to study the effect of the thickness of the sample on the cooling rate. The samples prepared with mould 2 measure 20 × 20 mm and have a thickness of 4 mm.

Macroscopically, all samples appear to be monolithic and homogeneous. The density of the bioaerogels as a function of the concentration of NFC is reported in Fig. 5. The theoretical density (continuous *black line* in Fig. 5) was calculated assuming no volume shrinkage from the gel to the dry sample. Aerogels have densities that vary between 0.012 and 0.043 g/cm^3. Their bulk density linearly increases with the concentration of NFC, which has already been described for cellulose and NFC aerogels [10, 22, 42, 43]. Porosities of the samples vary from 99% for the aerogels prepared from a 1% NFC suspension, to 98% for aerogels from a 3% NFC suspension. The density of aerogels is slightly higher than the theoretical one due to sample contraction during drying. Mould 1 produces the densest aerogels because the higher mould size results in greater shrinkage. However, even if the network is somewhat changed by the freeze-drying, this technique reaches very

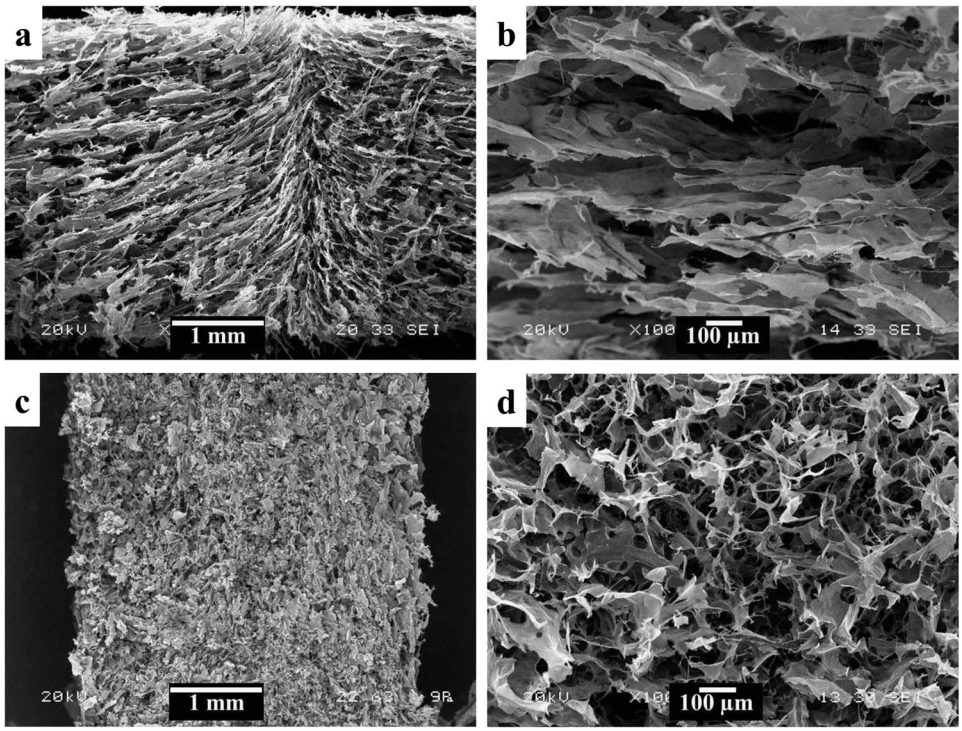

Fig. 6 Cross-section SEM images of aerogels prepared with **a**, **b** mould 1 and **c**, **d** mould 2

low-density values without undergoing significant shrinkage of the network.

3.3 Structural characterization of bioaerogels

Bioaerogels showed a 2D-sheet-like morphology (Fig. 6), which is commonly observed in the literature when NFC concentration exceeds 0.5 wt% [13, 22, 38, 44]. During the freezing step, fibres are separated from frozen water and confined to the interstitial regions, which causes an increase in the concentration between the ice crystals. When the concentration of NFC is higher than 0.5 wt%, the space available for the dispersion of the NFCs is restricted. Therefore, during the growth of crystals, the concentration of the NFC increases between the crystals and leads to the formation of a lamellar microstructure by aggregation of the fibres. When the freezing is complete, the frozen water is removed by sublimation. Hydrogen bonds and van der Waals forces hold the nanofibers together after the removal of water [45]. Thus, both aerogels showed a characteristic 2D-sheet-like morphology. The pore structure of aerogels obtained is a replica of the morphology of the ice crystals formed during the freezing process, and this structure ultimately depends upon the design of the sample holder (mould) and the resulting temperature gradient.

In the case of mould 1, this lamellar microstructure is oriented in the direction of the temperature gradient due to the anisotropic growth of the ice crystals [46]. The temperature gradient goes from each aluminium cover to the inside of the sample. It therefore crosses the aerogel horizontally. SEM images of the horizontal cross-sections of the aerogels produced in mould 1 are shown in Fig. 6a. In addition to the orientation of lamellae in the direction of the temperature gradient, three well-differentiated zones were distinguished. The freezing mechanism may explain the presence of these three areas. The complete freezing process can be divided into three stages: a solution cooling phase, a phase separation stage that comprises the primary and secondary nucleation of the ice and, finally, a frozen solution cooling stage [47]. During the cooling phase of the solution, heat conduction is the dominant heat transfer mechanism [48–50]. In the phase separation stage, the heat transfer by conduction and the latent heat released during a phase change are the main processes of heat exchange [47]. Primary nucleation occurs only once in regions those are in contact with the cold source. This is due to the release of latent heat caused by the formation of the first nuclei that prevents the nucleation of other nuclei in the other parts of the mould [51]. Consequently, the zone in contact with the aluminium (cold source) was characterized by a dense cellular microstructure with smaller randomly-distributed pores (Fig. 7a) [52]. During the crystal growth step, the solidification rate is subjected to the linear rate of crystallization [53]. The ice crystals gradually grow in the same direction as the temperature gradient and this directional solidification leads to a crystal alignment that leaves open pore channels after sublimation. (Fig. 7b). Similar zones have already been described for the ice-templating of

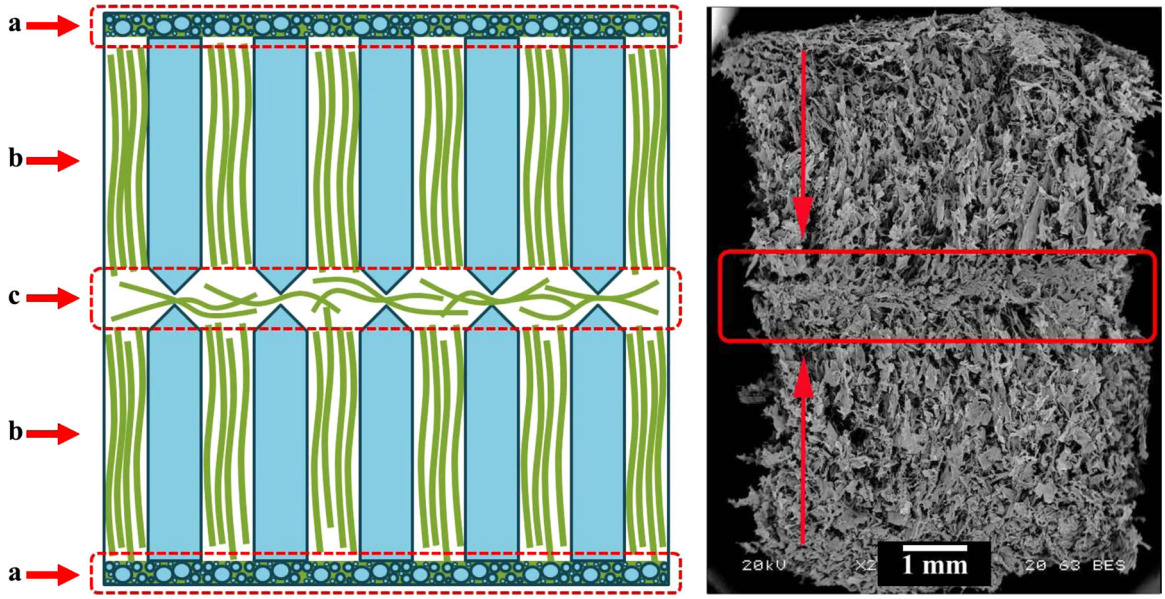

Fig. 7 Schematic diagram and cross-section SEM image of an aerogel showing the growth of ice crystals and a possible mechanism of formation of the three well-differentiated zones in aerogels prepared with mould 1. **a** Zone in contact with the aluminium, which is characterized by a dense cellular microstructure with smaller randomly-distributed pores; **b** Pore alignment along the temperature gradient and lamellar morphology; **c** Intermediate lamella from the aggregation of NFC pushed by opposite ice fronts. Arrows in the SEM image show the direction of growth of the water crystals and the intermediate layer is outlined in *red* (color figure online)

ceramic suspensions [46], cellulose scaffolds [54] and cellulose nanofibril foams [27]. Eventually, the crystal growth was terminated at the top of the suspension and formed a surface with a different microstructure [52]. This particular zone is formed because some nanofibers are pushed by ice fronts during crystal growth [55]. In our study, the temperature gradient was bidirectional (from both sides of the moulds) so that crystal growth occurs from both fronts that grow in the opposite direction of the cold source towards the interior of the aerogel. The NFCs pushed by each front of ice are trapped in the middle of the aerogel and also undergo an aggregation. This phenomenon creates an intermediate lamella that is observed by SEM at the centre of the formed aerogel (Fig. 7c). This separation zone constitutes a new geometry in the microstructure of aerogels.

In mould 2, as previously described, the temperature gradient was uniform throughout. This should lead to the ice crystals growing at the same rate in all directions, thus causing the formation, after sublimation, of a homogeneous distribution of pores within the resulting aerogel. Confirmation of this assumption was made by SEM examination of the aerogel produced in the mould (Fig. 6c). The cross-section revealed a dense cellular microstructure with randomly-distributed pores, and a multiple orientation of crystal growth was found.

Nitrogen adsorption was used to determine the specific surface area and porosity characteristics of the aerogels. There was no adsorption for either mould (Fig. 8a). The estimated specific surface area was around 1 m^2/g, which is characteristic of non-porous or macroporous solids. In order to compare the porosity of aerogels prepared from both moulds, the pore size was measured by analysis of SEM images. The pore size distribution obtained is represented in Fig. 8b.

The pore size distribution shows that about 65% of the pores are between 200 and 500 µm for aerogels prepared with mould 1. However, for aerogels prepared with mould 2, only about 65% of the pores are between 5 and 50 µm. The thickness of the sample plays an important role on the kinetics of ice formation, with higher cooling rates for thinner sample layers [22]. Consequently, freezing occurs more quickly in mould 2, which results in the formation of a greater number of nuclei. A large amount of crystal nuclei leads to faster global freezing and the formation of smaller crystals. After the sublimation of the frozen water, the crystals removed form the pores. Therefore, the aerogel microstructure has a smaller pore size. The effect of sample thickness on the kinetics of ice formation was studied in a previous work. It was shown that the spray freeze-drying technique leads to higher cooling rates, resulting in a significantly smaller pore size than in this study (40–70 nm) [12].

The properties of aerogels are a consequence of the distribution of their solid skeleton and their gaseous phase. The principal parameters characterizing the porous network of aerogels are the distribution of the pore size, their shape and the pore connectivity [56]. As indicated by the different microstructures found in this study, these parameters are

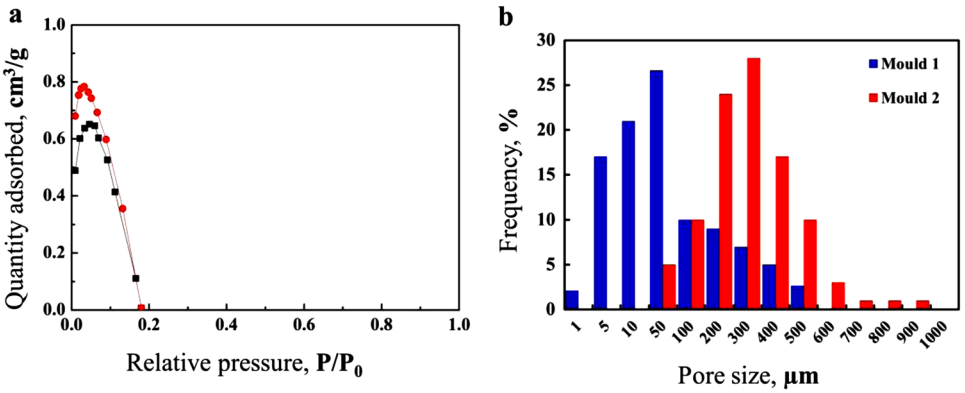

Fig. 8 **a** Typical nitrogen adsorption-desorption isotherm obtained for bioaerogels prepared by FD. **b** Pore size distributions of aerogels estimated by analysis of SEM images

highly influenced by the cooling rate. In order to highlight the correlation between the microstructure and the properties of aerogels, the thermal insulating properties of aerogels are described in the following section.

3.4 Thermal insulation properties of aerogels

The total thermal conductivity of aerogels was measured using the hot strip technique [38, 39]. Thermal conductivity values λ_{tot} of bioaerogels are given as a function of bulk density and are presented in Fig. 9.

The function of thermal insulating materials is to minimize the transport of heat through them. The heat transport in porous materials can be described by three factors: the conduction in solid phase, λ_{solid}; the conduction through gas phase, λ_{gas}; and the radiative heat transfer, λ_{rad}. These three thermal contributions are combined via radiation and conduction in order to calculate the total thermal conductivity. In this respect, the total equivalent thermal conductivity, λ_{tot}, of porous materials can be calculated by a parallel flux model [57]:

$$\lambda_{tot} = \lambda_{solid} + \lambda_{gas} + \lambda_{rad}$$

The influence of solid conduction on the total equivalent thermal conductivity notably increases with increasing density. In this work, aerogels reached very low-density values, reducing the contribution of solid conduction. The total thermal conductivity of aerogels varies because of the different microstructures obtained. Aerogels prepared with mould 1 have a 2D-sheet-like morphology with macropores, allowing the free circulation of air molecules and the conduction of heat as a result of the shock between air molecules. This lamellar microstructure also has a pore alignment along the temperature gradient that is applied during the freezing step and which leads to free circulation of thermal radiation. Thus, thermal radiation can easily pass through the aerogel without undergoing a significant attenuation. These types of aerogels were characterized by Pierre et al. [58] and the radiative heat transfer represents

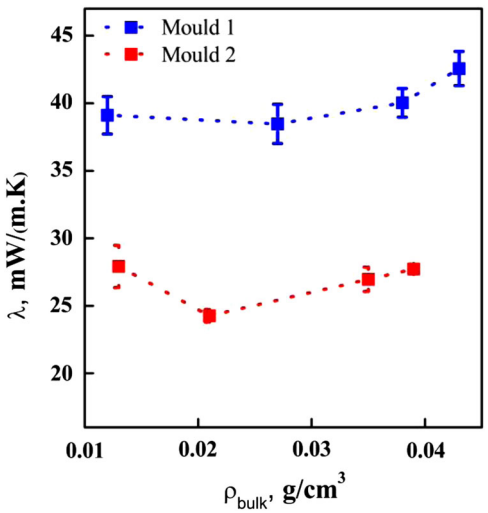

Fig. 9 Total thermal conductivity of bioaerogels as a function of bulk density. *Dotted lines* are guides for the eyes

about 48% of the total thermal conductivity. Therefore, bioaerogels obtained with mould 1 have high thermal conduction through the gas phase and high radiative heat transfer. As a consequence, they have the poorest performance in terms of thermal insulating properties, with a minimal thermal conductivity of 0.038 W/(m·K). Aerogels prepared with mould 2 also have a 2D-sheet-like morphology with macropores. In this case, the cellular microstructure has smaller randomly-distributed pores, but the contribution of gaseous conduction remains considerable since the Knudsen effect cannot be produced [59]. However, the absence of porous channels decreases the heat transfer by radiation. Aerogels behave as semi-transparent materials capable of absorbing, emitting and diffusing thermal radiation [60]. Absorption and diffusion induce the attenuation of radiation. Thus, the thermal insulating properties of aerogels obtained with mould 2 were improved compared to mould 1, and attain a minimal thermal conductivity of 0.024 W/(m·K).

4 Conclusion

Aerogels were prepared from NFC suspensions by freeze-drying using two different moulds in order to produce different freezing gradients to produce different pore organizations. Mould 1 was designed to induce a uniaxial temperature gradient in NFC suspensions during their freezing stage in order to maintain control of ice crystal growth. The subsequent freeze-drying process, in which the ice was sublimed, led to the formation of oriented pore channels. Conversely, mould 2 was designed to produce a uniform temperature gradient throughout the NFC suspension during freezing in order to obtain a smaller homogeneous distribution of pores and no pore alignment. This study shows that variations in the microstructures drastically affect the physico-chemical properties of the aerogels. Even with the same density and type of morphology, the orientation, shape and pore connectivity plays an essential role in the properties of aerogels. Aerogels prepared by freeze-drying in mould 2 have more efficient thermal insulating properties than aerogels prepared in mould 1. However, we demonstrated that temperature gradient can produce controlled anisotropic structures, which can be useful for other applications. The correlation between the microstructure and the properties of aerogels can therefore be used to design aerogels according to the desired application. In a previous study, the spray freeze-drying technique was presented as a new and effective method to prepare bioaerogels with thermal superinsulating properties [12]. In this study, we report that freeze-drying is a technique that allows the preparation of aerogels with a specific microstructure by adjusting the freezing rate. This parameter can be controlled by the size and materials of the mould and the creation of temperature gradients.

Acknowledgements This work was supported by the French Environment and Energy Management Agency (ADEME) and the Brittany region. The authors thank Anthony Magueresse (IRDL, UBS, Rue de Saint Maudé, Lorient, France) for the SEM images.

Compliance with ethical standards

Conflict of interest The authors declare that they have no competing interests.

References

1. Turbak AF, Snyder FW, Sandberg KR Microfibrillated cellulose, a new cellulose product: properties, uses, and commercial potential. In, 1983 1983. ITT Rayonier Inc., Shelton, WA
2. Herrick FW, Casebier RL, Hamilton JK, Sandberg KR Microfibrillated cellulose: morphology and accessibility. In, 1983 1983. ITT Rayonier Inc., Shelton, WA
3. Nechyporchuk O, Belgacem MN, Bras J (2016) Production of cellulose nanofibrils: a review of recent advances. Ind Crops Prod. doi:10.1016/j.indcrop.2016.02.016
4. Nogi M, Yano H (2008) Transparent nanocomposites based on cellulose produced by bacteria offer potential innovation in the electronics device industry. Adv Mater 20(10):1849–1852
5. Nogi M, Iwamoto S, Nakagaito AN, Yano H (2009) Optically transparent nanofiber paper. Adv Mater 21(16):1595–1598
6. Capadona JR, Shanmuganathan K, Tyler DJ, Rowan SJ, Weder C (2008) Stimuli-responsive polymer nanocomposites inspired by the sea cucumber dermis. Science 319(5868):1370–1374
7. Capadona JR, Van Den Berg O, Capadona LA, Schroeter M, Rowan SJ, Tyler DJ, Weder C (2007) A versatile approach for the processing of polymer nanocomposites with self-assembled nanofibre templates. Nat Nanotechnol 2(12):765–769
8. Walther A, Timonen JVI, Díez I, Laukkanen A, Ikkala O (2011) Multifunctional high-performance biofibers based on wet-extrusion of renewable native cellulose nanofibrils. Adv Mater 23(26):2924–2928
9. Shopsowitz KE, Qi H, Hamad WY, MacLachlan MJ (2010) Free-standing mesoporous silica films with tunable chiral nematic structures. Nature 468(7322):422–425
10. Kobayashi Y, Saito T, Isogai A (2014) Aerogels with 3D ordered nanofiber skeletons of liquid-crystalline nanocellulose derivatives as tough and transparent insulators. Angew Chem Int Ed 53 (39):10394–10397. doi:10.1002/anie.201405123
11. Pääkkö M, Vapaavuori J, Silvennoinen R, Kosonen H, Ankerfors M, Lindström T, Berglund LA, Ikkala O (2008) Long and entangled native cellulose I nanofibers allow flexible aerogels and hierarchically porous templates for functionalities. Soft Matter 4 (12):2492–2499. doi:10.1039/B810371B
12. Jiménez-Saelices C, Seantier B, Cathala B, Grohens Y (2017) Spray freeze-dried nanofibrillated cellulose aerogels with thermal superinsulating properties. Carbohyd Polym 157:105–113
13. Chen W, Li Q, Wang Y, Yi X, Zeng J, Yu H, Liu Y, Li J (2014) Comparative study of aerogels obtained from differently prepared nanocellulose fibers. ChemSusChem 7(1):154–161. doi:10.1002/cssc.201300950
14. Olsson RT, Samir MASA, Salazar-Alvarez G, Belova L, Ström V, Berglund LA, Ikkala O, Nogues J, Gedde UW (2010) Making flexible magnetic aerogels and stiff magnetic nanopaper using cellulose nanofibrils as templates. Nat Nanotechnol 5(8):584–588
15. Wang M, Anoshkin IV, Nasibulin AG, Korhonen JT, Seitsonen J, Pere J, Kauppinen EI, Ras RHA, Ikkala O (2013) Modifying native nanocellulose aerogels with carbon nanotubes for mechanoresponsive conductivity and pressure sensing. Adv Mater 25(17):2428–2432. doi:10.1002/adma.201300256
16. Hamedi M, Karabulut E, Marais A, Herland A, Nyström G, Wågberg L (2013) Nanocellulose aerogels functionalized by rapid layer-by-layer assembly for high charge storage and beyond. Angew Chem Int Ed 52(46):12038–12042. doi:10.1002/anie.201305137
17. Sehaqui H, Allais M, Zhou Q, Berglund LA (2011) Wood cellulose biocomposites with fibrous structures at micro- and nanoscale. Compos Sci Technol 71(3):382–387. doi:10.1016/j.compscitech.2010.12.007
18. Kocon L, Phalippou J (2005) Aérogels. Aspect matériau. Ed. Techniques Ingénieur
19. Sehaqui H, Salajková M, Zhou Q, Berglund LA (2010) Mechanical performance tailoring of tough ultra-high porosity foams prepared from cellulose I nanofiber suspensions. Soft Matter 6(8):1824–1832. doi:10.1039/b927505c
20. Donius AE, Liu A, Berglund LA, Wegst UGK (2014) Superior mechanical performance of highly porous, anisotropic nanocellulose–montmorillonite aerogels prepared by freeze casting. J Mech Behav Biomed Mater 37:88–99. doi:10.1016/j.jmbbm.2014.05.012

21. Svagan AJ, Samir MA, Berglund LA others (2008) Biomimetic foams of high mechanical performance based on nanostructured cell walls reinforced by native cellulose nanofibrils. Adv Mater 20 (7):1263
22. Aulin C, Netrval J, Wågberg L, Lindström T (2010) Aerogels from nanofibrillated cellulose with tunable oleophobicity. Soft Matter 6(14):3298–3305. doi:10.1039/C001939A
23. Jennings TA (1999) Lyophilization: introduction and basic principles. CRC Press
24. Deville S (2008) Freeze-casting of porous ceramics: a review of current achievements and issues. Adv Eng Mater 10(3):155–169. doi:10.1002/adem.200700270
25. Deville S, Saiz E, Tomsia AP (2007) Ice-templated porous alumina structures. Acta Mater 55(6):1965–1974. doi:10.1016/j.actamat.2006.11.003
26. Deville S (2010) Freeze-casting of porous biomaterials: structure, properties and opportunities. Materials 3(3):1913–1927
27. Martoïa F, Cochereau T, Dumont PJJ, Orgéas L, Terrien M, Belgacem MN (2016) Cellulose nanofibril foams: links between ice-templating conditions, microstructures and mechanical properties. Mater Des 104:376–391
28. Lee J, Deng Y (2011) The morphology and mechanical properties of layer structured cellulose microfibril foams from ice-templating methods. Soft Matter 7(13):6034–6040
29. Munier P, Gordeyeva K, Bergström L, Fall AB (2016) Directional freezing of nanocellulose dispersions aligns the rod-like particles and produces low-density and robust particle networks. Biomacromolecules 17(5):1875–1881. doi:10.1021/acs.biomac.6b00304
30. Stolze C, Janoschka T, Flauder S, Müller FA, Hager MD, Schubert US (2016) Investigation of ice-templated porous electrodes for application in organic batteries. ACS Appl Mater Interfaces 8 (36):23614–23623
31. Korhonen JT, Kettunen M, Ras RHA, Ikkala O (2011) Hydrophobic nanocellulose aerogels as floating, sustainable, reusable, and recyclable oil absorbents. ACS Appl Mater Interfaces 3 (6):1813–1816. doi:10.1021/am200475b
32. Kardam A, Raj KR, Srivastava S, Srivastava M (2014) Nanocellulose fibers for biosorption of cadmium, nickel, and lead ions from aqueous solution. Clean Technol Environ Policy 16 (2):385–393
33. Muzzarelli R, Baldassarre V, Conti F, Ferrara P, Biagini G, Gazzanelli G, Vasi V (1988) Biological activity of chitosan: ultrastructural study. Biomaterials 9(3):247–252
34. Rezwan K, Chen Q, Blaker J, Boccaccini AR (2006) Biodegradable and bioactive porous polymer/inorganic composite scaffolds for bone tissue engineering. Biomaterials 27(18):3413–3431
35. Saito T, Nishiyama Y, Putaux J-L, Vignon M, Isogai A (2006) Homogeneous suspensions of individualized microfibrils from TEMPO-catalyzed oxidation of native cellulose. Biomacromolecules 7(6):1687–1691
36. Ganster J, Fink HP (1999) Physical constants of cellulose. In: E.H. Immergut, & E.A. Grulke (eds) Polymer handbook. John Wiley and Sons edn., Wiley Database of Polymer Properties
37. Brunauer S, Emmett PH, Teller E (1938) Adsorption of gases in multimolecular layers. J Am Chem Soc 60(2):309–319
38. Bendahou D, Bendahou A, Seantier B, Grohens Y, Kaddami H (2015) Nano-fibrillated cellulose-zeolites based new hybrid composites aerogels with super thermal insulating properties. Ind Crops Prod 65:374–382. doi:10.1016/j.indcrop.2014.11.012
39. Gustafsson SE, Karawacki E, Khan MN (1979) Transient hot-strip method for simultaneously measuring thermal conductivity and thermal diffusivity of solids and fluids. J Phys D Appl Phys 12 (9):1411. doi:10.1088/0022-3727/12/9/003
40. Nijenhuis Kt, Mijs WJ (1998) Chemical and physical networks: formation and control of properties. vol 1, Wiley, Chichester [etc.]
41. Pääkkö M, Ankerfors M, Kosonen H, Nykänen A, Ahola S, Österberg M, Ruokolainen J, Laine J, Larsson PT, Ikkala O, Lindström T (2007) Enzymatic hydrolysis combined with mechanical shearing and high-pressure homogenization for nanoscale cellulose fibrils and strong gels. Biomacromolecules 8 (6):1934–1941. doi:10.1021/bm061215p
42. Sescousse R, Gavillon R, Budtova T (2011) Aerocellulose from cellulose–ionic liquid solutions: preparation, properties and comparison with cellulose–NaOH and cellulose–NMMO routes. Carbohyd Polym 83(4):1766–1774. doi:10.1016/j.carbpol.2010.10.043
43. Hoepfner S, Ratke L, Milow B (2008) Synthesis and characterisation of nanofibrillar cellulose aerogels. Cellulose 15 (1):121–129. doi:10.1007/s10570-007-9146-8
44. Silva TCF, Habibi Y, Colodette JL, Elder T, Lucia LA (2012) A fundamental investigation of the microarchitecture and mechanical properties of tempo-oxidized nanofibrillated cellulose (NFC)-based aerogels. Cellulose 19(6):1945–1956. doi:10.1007/s10570-012-9761-x
45. Hunter RJ (2001) Foundations of colloid science. Oxford University Press
46. Deville S, Saiz E, Tomsia AP (2006) Freeze casting of hydroxyapatite scaffolds for bone tissue engineering. Biomaterials 27 (32):5480–5489. doi:10.1016/j.biomaterials.2006.06.028
47. Yuan N-Y, Lin Y-A, Ho M-H, Wang D-M, Lai J-Y, Hsieh H-J (2009) Effects of the cooling mode on the structure and strength of porous scaffolds made of chitosan, alginate, and carboxymethyl cellulose by the freeze-gelation method. Carbohyd Polym 78 (2):349–356. doi:10.1016/j.carbpol.2009.04.021
48. Chen S-L, Lee T-S (1998) A study of supercooling phenomenon and freezing probability of water inside horizontal cylinders. Int J Heat Mass Transf 41(4):769–783
49. Yoon JI, Moon CG, Kim E, Son YS, Kim JD, Kato T (2001) Experimental study on freezing of water with supercooled region in a horizontal cylinder. Appl Therm Eng 21(6):657–668
50. Zhang H, Hussain I, Brust M, Butler MF, Rannard SP, Cooper AI (2005) Aligned two-and three-dimensional structures by directional freezing of polymers and nanoparticles. Nat Mater 4 (10):787–793
51. Pawelec KM, Husmann A, Best SM, Cameron RE (2014) Understanding anisotropy and architecture in ice-templated biopolymer scaffolds. Mater Sci Eng C 37:141–147. doi:10.1016/j.msec.2014.01.009
52. Dash R, Li Y, Ragauskas AJ (2012) Cellulose nanowhisker foams by freeze casting. Carbohyd Polym 88(2):789–792. doi:10.1016/j.carbpol.2011.12.035
53. Budiaman ER, Fennema O (1987) Linear rate of water crystallization as influenced by temperature of hydrocolloid suspensions. J Dairy Sci 70(3):534–546
54. Flauder S, Heinze T, Müller FA (2014) Cellulose scaffolds with an aligned and open porosity fabricated via ice-templating. Cellulose 21(1):97–103. doi:10.1007/s10570-013-0119-9
55. Han J, Zhou C, Wu Y, Liu F, Wu Q (2013) Self-assembling behavior of cellulose nanoparticles during freeze-drying: effect of suspension concentration, particle size, Crystal structure, and surface charge. Biomacromolecules 14(5):1529–1540. doi:10.1021/bm4001734
56. Reichenauer G (2008) Aerogels. In: Arza Seidel & Mickey Bickford (eds) Kirk-othmer encyclopedia of chemical technology. John Wiley & Sons, Inc
57. Ebert H-P (2011) Thermal properties of aerogels. In: Aegerter MA, Leventis N, & Koebel MM (eds) Aerogels handbook. Advances in sol-gel derived materials and technologies. Springer, New York, p 537–564
58. Pierre T, Jiménez-Saelices C, Seantier B, Grohens Y (2017) Transient pulsed technique to characterize the radiative and

conductive properties of bio aerogels. Accepted for publication in Int J Therm Sci
59. Kaganer MG (1969) Thermal Insulation in Cryogenic Engineering. Israel Program for Scientific Translations (1969) Jerusalem
60. Wei G, Liu Y, Zhang X, Du X (2013) Radiative heat transfer study on silica aerogel and its composite insulation materials. J Non-Cryst Solids 362:231–236. doi:10.1016/j.jnoncrysol.2012.11.041